IET Power Electronics

Research Article

IET Journals
The Institution of Engineering and Technology

Power oscillation analysis and control of three-phase grid-connected voltage source converters under unbalanced grid faults

ISSN 1755-4535
Received on 7th October 2015
Revised on 6th March 2016
Accepted on 5th May 2016
doi: 10.1049/iet-pel.2015.0804
www.ietdl.org

Xiong Du[1] ✉, Yue Wu[1], Shida Gu[1], Heng-Ming Tai[2], Pengju Sun[1], Yongliang Ji[3]

[1]*State Key Laboratory of Power Transmission Equipment and System Security and New Technology, Chongqing University, Chongqing 400044, People's Republic of China*
[2]*Department of Electrical and Computer Engineering, University of Tulsa, Tulsa, OK 74104, USA*
[3]*Electric Power Research Institute of State Grid Chongqing Electric Power Company, Chongqing 404000, People's Republic of China*
✉ *E-mail: duxiong@cqu.edu.cn*

Abstract: Control of three-phase grid-connected voltage source converter under unbalanced grid faults greatly depends on the active and reactive powers processed by the converter. The instantaneous active power theory with sequence decomposition is employed to analyse the instantaneous power components, especially the second-order oscillation power. Study shows that the second-order oscillation power comprises two quadrature components, the cosine and sine terms, which are contributed by the average active power and the average reactive power, respectively. This finding sheds insight on the regulation of oscillation power under unbalanced grid conditions. Based on this observation, the authors propose a positive and negative sequence conductance and susceptance control scheme, which enables simple regulation of the active power or reactive power oscillation with the average active power and reactive power control. In addition, the authors investigate the relationship between the positive/negative sequence conductance and susceptance distribution factors with power oscillation and peak current. A maximum current limitation scheme is embedded into the current reference generation block for overcurrent protection. Numerical simulations and prototype measurements verify the accuracy of the analysis and the effectiveness of the control scheme.

1 Introduction

Three-phase grid-connected voltage source converters (VSC) are widely used in the front-end rectifier, renewable energy integration, and distributed generation fields [1–4]. The control of three-phase VSC for unbalanced grid has drawn much attention due to the fault-ride through requirement for grid safety under such grid condition [2, 5–7]. In the balanced grid condition, the three-phase voltage has a symmetrical positive-sequence voltage dip, whereas under an unbalanced grid fault, in addition to the positive-sequence voltage dip, the negative-sequence component in the grid voltage also exists [5, 8].

Most production-grade VSCs employ the balanced positive-sequence (BPS) current control under unbalanced grid condition [3], as specified in the grid codes [6, 7]. Through such control scheme, the negative sequence voltage in the grid voltage could not be compensated without the negative sequence reactive power. Moreover, even the grid side currents are positive sequence balanced, the interaction between the positive sequence current and the negative sequence voltage still generates the second order active power oscillation. This active power oscillation will introduce the second order voltage ripple in the dc bus voltage. This dc bus ripple, in turn, results in the instantaneous overvoltage which may damage the semiconductor devices in VSC [5]. This second order voltage ripple in the dc bus, at the same time, will generate undesired third-order current harmonic in the grid side. These third-order current harmonic will introduce the power quality problem [9]. Converter tripping due to overvoltage or overcurrent may occur without proper control. Although control of the grid-connected VSC has been developed in industry, only the BPS power injection is adopted as required in the grid codes [10]. Based on a new grid code draft published in 2012, the transmission system operator may propose the requirement for unbalanced current injection employing the positive-sequence and the negative-sequence [10, 11].

Some researchers have presented approaches to deal with the converter control issue under unbalanced grid fault conditions [12–24]. Five active power control methods have been presented in [12]: they are the instantaneous active reactive control, instantaneously controlled positive-sequence, positive–negative-sequence compensation (PNSC), average active-reactive control (AARC), and the balanced positive-sequence control. Compact expressions of the above control schemes were presented in [13] with proper selection variables. The first two control schemes generate current harmonics and the other three methods inject sinusoidal current to the grid. Current controllers based on symmetrical components and linear quadratic regulators were considered in [14]. Control of the positive-sequence and negative-sequence reactive power for grid supporting was discussed in [10, 15–17]. Moreover, the upper and lower phase voltage limits were considered in [15, 16]. How to realise the maximum reactive current injection for the lowest amplitude common coupling point (PCC) phase voltage when considering the overvoltage for the largest amplitude PCC phase voltage was investigated in [17]. The individual phase voltage support was investigated in [10], while the voltage support problem for low voltage systems was addressed in [18].

Unbalanced current leads to difficulty on over-current limitation. A current reference generator for positive-sequence and negative-sequence current injection with peak current limitation has been designed, while the effects of the active power and reactive power fluctuation were not addressed [3]. The harmonic current is injected to reduce the phase current [20], and zero-sequence components have been employed to realise the phase current distribution in a three-phase four-wire system [21]. For the active power oscillation reduction, appropriate current

harmonics can be injected to minimise the active power ripple [22]. Some control schemes through introduced regulation parameters to the positive-sequence and negative-sequence voltage or power were discussed in [23, 24]. Both of the active power and reactive power ripples can be controlled, but the current limitation is not considered in these methods.

Instantaneous power analysis is one of the basics of the converter control under grid fault condition. The average active power and reactive power have been well studied, and the oscillation in the instantaneous active power and reactive power also have been widely discussed and considered as one of the control targets [1, 3, 5, 15, 24]. However, the relationships between the average power and oscillation power, and the interaction of the positive-sequence and negative-sequence voltage and current have not been well reported.

In this paper we intend to investigate the instantaneous active power and reactive power processed by VSC in a rigorous manner. We find that the active and reactive oscillation power consists of two orthogonal components, which can be determined by the average active and reactive power independently. Based on the decoupling effect of average active power and reactive power to the oscillation power, a positive and negative sequence conductance and susceptance (PNGB) control scheme is proposed for the grid fault control. Analytical relations between the control parameters of conductance and susceptance with the power oscillation amplitude and peak phase current are derived. The PNGB method can regulate the average active power and reactive power with flexible control of the active and reactive power oscillation. A current limitation block is inserted into the control loop for over-current prevention. The novelty is that the proposed method is capable of achieving power oscillation regulation and current limitation at the same time when both injection of active power and reactive power are available under unbalanced grid condition.

This paper is organised as follows. Section 2 investigates the power oscillation characteristics. The proposed PNGB control method is presented in Section 3, so is the analytical analysis. Section 4 shows the numerical and experimental results that validate the effectiveness of the proposed control scheme. The reactive power output capability of the PNGB control scheme is discussed in Sections 5 and 6 concludes this paper.

2 Power oscillation analysis under unbalanced grid faults

This section will analyse the active and reactive power components, especially the power oscillation components in detail. The results can be used as a guideline for proper design of control strategies under unbalanced grid conditions.

The three-phase grid-connected VSC under analysis is shown in Fig. 1. The dc bus of VSC is fed by an upstream converter or a dc source such as a PV panel or a battery pack. The grid-connected VSC is a three-phase three-wire inverter connected to the grid at the PCC. The grid is equivalent to a voltage source $\boldsymbol{v}_{\mathbf{g}}$ in series with equivalent inductors L_g. Under unbalanced grid fault condition, the voltage $\boldsymbol{v}$ at PCC and the grid current $\boldsymbol{i}$ will contain both the positive-sequence and the negative-sequence components. The zero-sequence component can be neglected due to the three-wire structure. The electrical notations are shown in Table 1.

The three-phase voltage $\boldsymbol{v}$ at PCC can be expressed in the complex-valued form with positive-sequence and negative-sequence components [25],

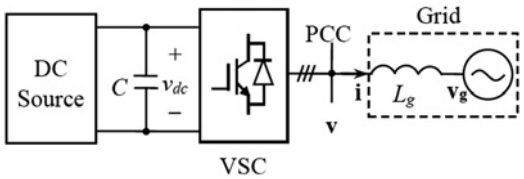

Fig. 1 *Diagram of a three-phase grid-connected VSC*

$$\boldsymbol{v} = \boldsymbol{v}^+ + \boldsymbol{v}^- = V^+ e^{j(\omega_0 t + \phi_v^+)} + V^- e^{j(-\omega_0 t + \phi_v^-)} \tag{1}$$

$$\boldsymbol{i} = \boldsymbol{i}^+ + \boldsymbol{i}^- = I^+ e^{j(\omega_0 t + \phi_i^+)} + I^- e^{j(-\omega_0 t + \phi_i^-)} \tag{2}$$

where V^+ and V^- are amplitudes of the positive sequence and negative sequence voltages, respectively, I^+ and I^- are amplitudes of the positive-sequence and negative-sequence currents. φ_v^+, φ_v^-, φ_i^+, and φ_i^- are the corresponding phase angles, and ω_0 is the angular frequency of the grid voltage.

Further, the positive and negative sequence currents can be divided into the active power and reactive power components,

$$\boldsymbol{i}^+ = \boldsymbol{i}_p^+ + \boldsymbol{i}_q^+ \tag{3}$$

$$\boldsymbol{i}^- = \boldsymbol{i}_p^- + \boldsymbol{i}_q^-, \tag{4}$$

where $\boldsymbol{i}_p^+$ and $\boldsymbol{i}_p^-$ are in phase with $\boldsymbol{v}^+$ and $\boldsymbol{v}^-$,while $\boldsymbol{i}_q^+$ and $\boldsymbol{i}_q^-$ lag $\boldsymbol{v}^+$ and $\boldsymbol{v}^-$ by 90°, respectively. The relationship between $\boldsymbol{v}$ and $\boldsymbol{i}$ can be expressed with the conductance and susceptance as

$$\boldsymbol{i}_p^+ = g^+ \boldsymbol{v}^+ \tag{5}$$

$$\boldsymbol{i}_p^- = g^- \boldsymbol{v}^- \tag{6}$$

$$\boldsymbol{i}_q^+ = -jb^+ \boldsymbol{v}^+ \tag{7}$$

$$\boldsymbol{i}_q^- = -jb^- \boldsymbol{v}^- \tag{8}$$

where g^+ and g^- are, respectively, the positive sequence and negative sequence conductance, b^+ and b^- are the positive sequence and negative sequence susceptance.

The instantaneous active power p and reactive power q can be obtained by [25]

$$p + jq = \boldsymbol{v} \cdot \boldsymbol{i}^*. \tag{9}$$

Table 1 Electrical notations

Symbol	Physical meaning
$\boldsymbol{v}_{\mathbf{g}}$	grid voltage
$\boldsymbol{v}$	voltage at PCC
$\boldsymbol{v}^+$, $\boldsymbol{v}^-$	positive and negative sequence voltage at PCC
V^+, V^-	amplitude of the positive and negative sequence voltage at PCC
$\boldsymbol{i}$, $\boldsymbol{i}_{\mathbf{ref}}$	grid current and grid current reference
I_{max}	maximum amplitude of phase currents
I_{lim}	phase current limitation value
$\boldsymbol{i}^+$, $\boldsymbol{i}^-$	positive and negative sequence grid current
I^+, I^-	amplitude of the positive and negative sequence grid current
$\boldsymbol{i}_p^+$, $\boldsymbol{i}_q^+$, $\boldsymbol{i}_p^-$, $\boldsymbol{i}_q^-$	active power and reactive power components of positive and negative sequence grid current
g^+, g^-	positive sequence and negative sequence conductance
b^+, b^-	positive sequence and negative sequence conductance
p, q	instantaneous active and reactive power
P, Q, $\tilde{p}$, $\tilde{q}$	dc and ac components of instantaneous active and reactive power
Δp, Δq	amplitude of $\tilde{p}$, $\tilde{q}$
p_{cos}, p_{sin}, q_{cos}, q_{sin} Δp_{cos}, Δp_{sin}, Δq_{cos}, Δq_{sin}	cosine and sine components in $\tilde{p}$ and $\tilde{q}$ amplitude of p_{cos}, p_{sin}, q_{cos}, q_{sin}

Equation (9) can be expressed in the form

$$p = \mathrm{Re}\Big\{\boldsymbol{v}^+ \cdot (\boldsymbol{i}_p^+)^* + \boldsymbol{v}^+ \cdot (\boldsymbol{i}_p^-)^* + \boldsymbol{v}^+ \cdot (\boldsymbol{i}_q^+)^* + \boldsymbol{v}^+ \cdot (\boldsymbol{i}_q^-)^* + \boldsymbol{v}^- \cdot (\boldsymbol{i}_p^+)^* + \boldsymbol{v}^- \cdot (\boldsymbol{i}_p^-)^* + \boldsymbol{v}^- \cdot (\boldsymbol{i}_q^+)^* + \boldsymbol{v}^- \cdot (\boldsymbol{i}_q^-)^*\Big\} \quad (10)$$

$$q = \mathrm{Im}\Big\{\boldsymbol{v}^+ \cdot (\boldsymbol{i}_p^+)^* + \boldsymbol{v}^+ \cdot (\boldsymbol{i}_p^-)^* + \boldsymbol{v}^+ \cdot (\boldsymbol{i}_q^+)^* + \boldsymbol{v}^+ \cdot (\boldsymbol{i}_q^-)^* + \boldsymbol{v}^- \cdot (\boldsymbol{i}_p^+)^* + \boldsymbol{v}^- \cdot (\boldsymbol{i}_p^-)^* + \boldsymbol{v}^- \cdot (\boldsymbol{i}_q^+)^* + \boldsymbol{v}^- \cdot (\boldsymbol{i}_q^-)^*\Big\}. \quad (11)$$

Substituting (5)–(8) into (10) and (11) yields the expressions of active power and reactive power components generated by the positive and negative sequence voltages and currents, which are shown in Table 2. It can be seen from Table 2 that both the active power and reactive power contains dc components and oscillation components under unbalanced conditions such that

$$p = P + \tilde{p} \quad (12)$$

$$q = Q + \tilde{q}. \quad (13)$$

The dc and oscillation components are

$$P = \frac{3}{2} g^+ (V^+)^2 + \frac{3}{2} g^- (V^-)^2 \quad (14)$$

$$Q = \frac{3}{2} b^+ (V^+)^2 + \frac{3}{2} b^- (V^-)^2 \quad (15)$$

$$\tilde{p} = \frac{3}{2} V^+ V^- \big[(g^+ + g^-)\cos(2\omega t + \varphi_v^+ - \varphi_v^-) + (b^+ - b^-)\sin(2\omega t + \varphi_v^+ - \varphi_v^-)\big] \quad (16)$$

$$\tilde{q} = \frac{3}{2} V^+ V^- \big[(b^+ + b^-)\cos(2\omega t + \varphi_v^+ - \varphi_v^-) + (g^- - g^+)\sin(2\omega t + \varphi_v^+ - \varphi_v^-)\big]. \quad (17)$$

The dc component P in the instantaneous active power p denotes the average active power transferred from the dc link to ac grid [25]; thus regulating the conductance g^+ and g^- enables the control of the average active power P. In a similar manner, the dc component Q in q can be regulated by controlling the susceptance b^+ and b^-. The average dc components, P and Q, have been investigated in the literatures [1, 3, 5, 10, 11]. It is observed from (16) and (17) that the oscillation components contain the second harmonics in-phase and quadrature components. For example, consider the active power oscillation component,

$$\tilde{p} = p_{\cos} + p_{\sin} \quad (18)$$

$$p_{\cos} = \frac{3}{2} V^+ V^- (g^+ + g^-)\cos(2\omega t + \varphi_v^+ - \varphi_v^-) \quad (19)$$

$$p_{\sin} = \frac{3}{2} V^+ V^- (b^+ - b^-)\sin(2\omega t + \varphi_v^+ - \varphi_v^-). \quad (20)$$

Due to the orthogonal characteristics of the cosine and the sine terms, it follows from (19) and (20) that the average active power and reactive power determine the active power ripple, but with no coupling. Reducing the amplitude of the cosine term and/or the sine term lowers the total active power ripple. Thus the active power oscillation can be regulated via the control of g^+ with g^- and b^+ with b^- independently or together. Similar conclusion can be drawn for the reactive power oscillation. However, the conductance and susceptance may have opposite effects on the active power ripple and reactive power ripple. For example, the sum of the conductance $(g^+ + g^-)$ may be small which reduces $p_{\cos}$, but the difference $(g^- - g^+)$ may be large and leads to the increase of the $q_{\sin}$ term.

On the basis the above analysis of power oscillation under the grid fault condition, in particular, the orthogonal characteristics of the oscillation power with decoupling performance, a positive sequence and negative sequence conductance and susceptance control scheme will be proposed in the next section to regulate the dc component and the oscillation components in the active power and the reactive power.

3 PNGB control scheme

In unbalanced grid fault condition, VSC should ride-through the fault with the new grid code. Hence the average active power and reactive power, P and Q, will be set as the reference for VSC control. How to formulate the current reference according to the PQ reference has drawn a great deal of attention in the power electronics field [1, 3, 5, 12, 15, 23, 24]. This section proposes a current reference generation scheme based on regulating the proportion between the positive-sequence and negative-sequence conductance and susceptance. The proposed method not only can realise the required average power output, but also can regulate the power oscillation.

3.1 Positive and negative sequence conductance and susceptance method

The active power and reactive power current references are set by the corresponding conductance and susceptance. Let the proportion between the positive sequence and negative sequence conductance and susceptance be

$$g^- = k_G g^+ \quad (21)$$

$$b^- = k_B b^+. \quad (22)$$

The physical meaning of the proportionality factors k_G and k_B are the proportion between the negative sequence conductance and susceptance to the respective positive sequence ones. Then the current reference can be obtained as

$$\boldsymbol{i}_{\mathrm{ref}} = g^+ \boldsymbol{v}^+ + k_G g^+ \boldsymbol{v}^- - j b^+ \boldsymbol{v}^+ - j k_B b^+ \boldsymbol{v}^-. \quad (23)$$

Theoretically, k_G and k_B can be any real numbers. However, the values of k_G and k_B will affect the power ripple as well as the peak of phase currents. The selection criteria of these values are discussed in the following and based on the analysis of the power ripple and peak current.

When k_G and k_B are selected, the corresponding conductance g^+ and g^- can be determined according to the given PQ reference

$$g^+ = \frac{2}{3} \frac{P}{(V^+)^2 + k_G (V^-)^2} \quad (24)$$

$$b^+ = \frac{2}{3} \frac{Q}{(V^+)^2 + k_B (V^-)^2}. \quad (25)$$

Different k_G and k_B values give different control schemes. For $k_G = 0$ or $k_B = 0$, the control scheme is equivalent to the BPS control [12]. For $k_G = 1$ or $k_B = 1$, the control scheme corresponds to the existing AARC [12]. For $k_G = -1$ or $k_B = -1$, the control scheme is equivalent to the PNSC control [12]. Other values of k_G and k_B produce different control effects with distinct power ripple and phase current.

IET Power Electron., 2016, Vol. 9, Iss. 11, pp. 2162–2173

Table 2 Relationships between power and current components

	Active power current		Reactive power current	
	i_p^+	i_p^-	i_q^+	i_q^-
P	$\frac{3}{2}g^+(V^+)^2$	$\frac{3}{2}g^-(V^-)^2$	0	0
Q	0	0	$\frac{3}{2}b^+(V^+)^2$	$\frac{3}{2}b^-(V^-)^2$
$\tilde{p}$	$\frac{3}{2}g^+V^+V^-\cos(2\omega t+\varphi_v^+-\varphi_v^-)$	$\frac{3}{2}g^-V^+V^-\cos(2\omega t+\varphi_v^+-\varphi_v^-)$	$\frac{3}{2}b^+V^+V^-\sin(2\omega t+\varphi_v^+-\varphi_v^-)$	$-\frac{3}{2}b^-V^+V^-\sin(2\omega t+\varphi_v^+-\varphi_v^-)$
$\tilde{q}$	$-\frac{3}{2}g^+V^+V^-\sin(2\omega t+\varphi_v^+-\varphi_v^-)$	$\frac{3}{2}g^-V^+V^-\sin(2\omega t+\varphi_v^+-\varphi_v^-)$	$\frac{3}{2}b^+V^+V^-\cos(2\omega t+\varphi_v^+-\varphi_v^-)$	$\frac{3}{2}b^-V^+V^-\cos(2\omega t+\varphi_v^+-\varphi_v^-)$

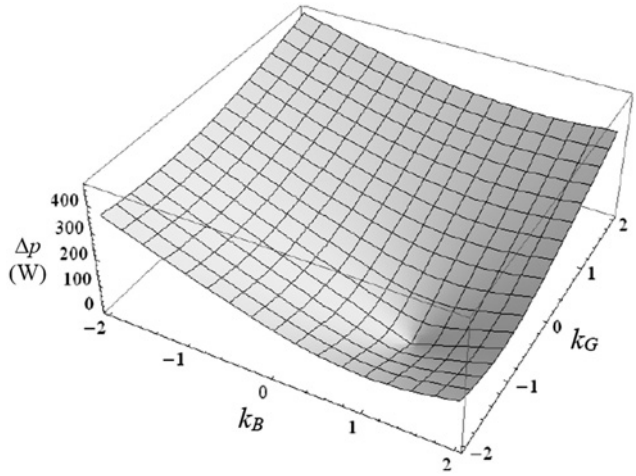

Fig. 2 *Δp as a function of k_G and k_B*

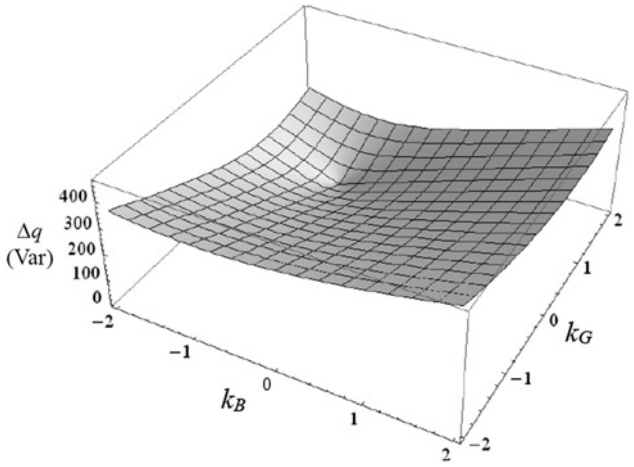

Fig. 3 *Δq as a function of k_G and k_B*

3.2 Power ripple and peak current analysis

It follows from (16) and (17) that amplitudes of the active power and reactive power ripples are

$$\Delta p=\sqrt{\Delta p_{\cos}^2+\Delta p_{\sin}^2}=\frac{3}{2}V^+V^-\sqrt{(g^+)^2(1+k_G)^2+(b^+)^2(1-k_B)^2} \tag{26}$$

$$\Delta q=\sqrt{\Delta q_{\cos}^2+\Delta q_{\sin}^2}=\frac{3}{2}V^+V^-\sqrt{(g^+)^2(1-k_G)^2+(b^+)^2(1+k_B)^2}. \tag{27}$$

where $\Delta p_{\cos}$, $\Delta p_{\sin}$, $\Delta q_{\cos}$, and $\Delta q_{\sin}$ are the amplitudes of the cosine term and the sine term of active power and reactive power ripples, respectively. At a grid fault condition where phase a has a single-phase grounded fault, the phase voltage decreases to 70% of the normal voltage of 110 V rms. At this condition, when $P=1000$ W and $Q=1000$ Var, the amplitude of active power ripple Δp and that of reactive power ripple Δq versus k_G and k_B are illustrated in Figs. 2 and 3, respectively.

With numerical calculation and the view from Fig. 2, when $k_G=-1$ and $k_B=1$, $\Delta p=0$, while $\Delta q=314.3$ Var. Similarly, from Fig. 3, when $k_G=1$ and $k_B=-1$, $\Delta q=0$ and $\Delta p=314.3$ W. It is obvious that different combinations of k_G and k_B lead to different values of Δp and Δq. In the view of minimising Δp, $k_G=-1$, and $k_B=1$, while in the view of minimising Δq, $k_G=1$ and $k_B=-1$. However, different values of k_G and k_B also affect the peak value of phase current. These characteristics with a few groups of typical k_G and k_B are summarised in Table 3.

Under unbalanced condition, the phase currents are unbalanced and may have different amplitudes, the phase current i_a, i_b and i_c can be expressed as

$$i_a=\sqrt{(g^+)^2+(b^+)^2}V^+\cos(\omega t+\varphi_v^++\theta^+)+\sqrt{(k_Gg^+)^2+(k_Bb^+)^2}V^-\cos(-\omega t+\varphi_v^-+\theta^-) \tag{28}$$

$$i_b=\sqrt{(g^+)^2+(b^+)^2}V^+\cos\left(\omega t+\varphi_v^++\theta^+-\frac{2\pi}{3}\right)+\sqrt{(k_Gg^+)^2+(k_Bb^+)^2}V^-\cos\left(-\omega t+\varphi_v^-+\theta^--\frac{2\pi}{3}\right) \tag{29}$$

$$i_c=\sqrt{(g^+)^2+(b^+)^2}V^+\cos\left(\omega t+\varphi_v^++\theta^++\frac{2\pi}{3}\right)+\sqrt{(k_Gg^+)^2+(k_Bb^+)^2}V^-\cos\left(-\omega t+\varphi_v^-+\theta^-+\frac{2\pi}{3}\right) \tag{30}$$

where $\theta^+=\arg(g^+-jb^+)$ and $\theta^-=\arg(g^--jb^-)$.

Then the amplitude of each phase current can be expressed as (see equation 31, (32) (33) at bottom of next page)

where $\phi_i^a=\phi_v^++\theta^++\phi_v^-+\theta^-$, $\phi_i^b=\phi_i^a+2\pi/3$, and $\phi_i^c=\phi_i^a-2\pi/3$.

$$I_{amp}=\sqrt{\left[(g^+)^2+(b^+)^2\right](V^+)^2+\left[(k_Gg^+)^2+(k_Bb^+)^2\right](V^-)^2+2\sqrt{(g^+)^2+(b^+)^2}\sqrt{(k_Gg^+)^2+(k_Bb^+)^2}V^+V^-\cos(\varphi_i^a)} \tag{31}$$

Table 3 Power oscillation and peak current with different k_G and k_B

k_G	k_B	Δp, W	Δq, Var	I_{max}, A
−1	1	0	314.3	7.48
1	−1	314.3	0	7.14
0	0	157.1	157.1	6.73
1	1	219.5	219.5	7.3

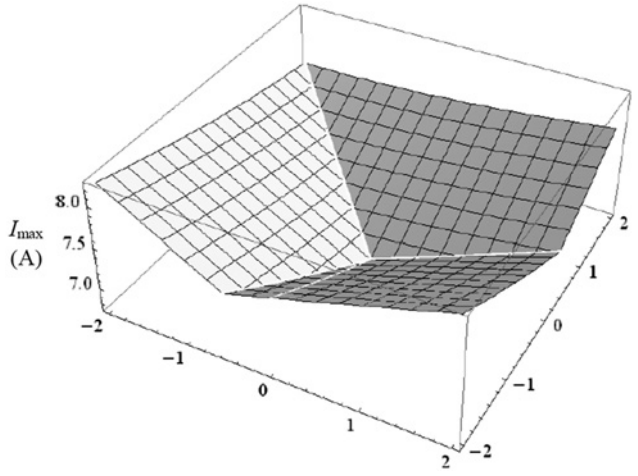

Fig. 4 *Peak current I_{max} as a function of k_G and k_B*

Since phase currents are different, the maximum phase current can be defined as the maximum among the phase current amplitudes

$$I_{\max} = \max(I_{amp}, I_{bmp}, I_{cmp}). \tag{34}$$

Then the overcurrent limitation can be realised according to $I_{\max}$, instead of the amplitude of phase current. The maximum phase current $I_{\max}$ as a function of k_G and k_B is displayed in Fig. 4.

As depicted in Fig. 4, the peak value of the phase current largely depends on the values of k_G and k_B. Numerical calculation shows that the minimum of $I_{\max}$ is 6.73 A, which occurs at $k_G = 0$ and $k_B = 0$. As will be shown in Table 3, Δp, Δq, and $I_{\max}$ may not reach the minima all at the same time with specific values of k_G and k_B. Hence the selection of k_G and k_B values involves with the tradeoff between Δp or Δq and $I_{\max}$.

When k_G and k_B are selected according to the given average power, P and Q, a maximum phase current $I_{\max}$ larger than the current limitation value $I_{\lim}$ may occur due to the constraints of Δp and Δq. Therefore, an overcurrent limitation scheme described below is added in the control loop to prevent this situation.

3.3 Maximum current limitation scheme

Given the values of P, Q, k_G, and k_B, the conductance and susceptance can be calculated from (24) and (25). The calculated conductance and susceptance are denoted as g^+_{cal} and b^+_{cal}, respectively. Then the maximum phase current $I_{\max}$ can be calculated by (34). For a specific VSC, set the affordable maximum phase current as $I_{\lim}$. The current limitation is realised through clamping the conductance and susceptance to prevent the peak phase current from over $I_{\lim}$

$$g^+ = \begin{cases} g^+_{\text{cal}}, I_{\max} \le I_{\lim} \\ \dfrac{I_{\lim}}{I_{\max}} g^+_{\text{cal}}, I_{\max} > I_{\lim} \end{cases} \tag{35}$$

$$b^+ = \begin{cases} b^+_{\text{cal}}, I_{\max} \le I_{\lim} \\ \dfrac{I_{\lim}}{I_{\max}} b^+_{\text{cal}}, I_{\max} > I_{\lim}. \end{cases} \tag{36}$$

When the calculated peak current $I_{\max}$ is smaller than $I_{\lim}$, the overcurrent scheme is bypassed. If the calculated $I_{\max}$ is larger than $I_{\lim}$, the current decreases proportionally along with ($I_{\lim}/I_{\max}$). This scheme guarantees the prevention of overcurrent and the maximum peak phase current equal to $I_{\lim}$.

The current reference generation scheme with current limitation is implemented by the block diagram in Fig. 5. As shown in Fig. 5, the grid voltage $\boldsymbol{v}$ passes through a sequential extraction block to obtain the positive sequence and the negative sequence components, $\boldsymbol{v}^+$ and $\boldsymbol{v}^-$. This block is essentially a double second order generalised integrator PLL [26]. Together with P, Q, k_G, and k_B, the peak current $I_{\max}$ is obtained via (34). The current limitation block takes $I_{\max}$ and $I_{\lim}$ as the inputs to generate g^+ and b^+ via (35) and (36). Then the current reference $\boldsymbol{i}_{\text{ref}}$ is generated via the reference generation block. The current controller generates the driving signals of VSC by $\boldsymbol{i}_{\text{ref}}$ and the grid current $\boldsymbol{i}$. As indicated by Fig. 5, only $I_{\lim}$ is required to be selected for the design of the current limitation function. This design parameter is usually determined by the current rating of the semiconductor device employed in the VSC. In order to test the current limitation function, $I_{\lim}$ is set to 5 A in this study.

Although the analytical expression of power oscillation and maximum current have been obtained, it is still difficult to analytically determine the value of the k_G and k_B, since the values of k_G and k_B are related to Δp, Δq, and $I_{\max}$; and the relationship is not monotonic. The k_G and k_B should be carefully selected considering the specific requirements in practice.

3.4 Performance comparison

Several power control techniques have been reported in the literatures. Performance comparisons in terms of the regulation of average active and reactive power, the capability of current and grid voltage limitation, and the regulation of active and reactive power fluctuations $\tilde{p}$, $\tilde{q}$ of these techniques are presented in Table 4.

Many studies on regulation of active power P or reactive power Q, or both of P and Q, by generating the positive sequence and negative sequence active current references have been reported [3, 12, 13, 15–17, 23, 24]. Five different active power control methods were proposed in [12], but the current limitation, grid voltage limitation and control of $\tilde{p}$, $\tilde{q}$ were not discussed. In [13], control parameters α and β were selected to regulate the active power P and power oscillations $\tilde{p}$, $\tilde{q}$. The current and grid voltage limits have been considered to realise the maximum reactive power injection when only reactive power was injected under grid fault, but the control of $\tilde{p}$, $\tilde{q}$ was not examined [16, 17]. Other reports investigated simultaneous regulation of P and Q [3, 15, 23, 24], including the work of this paper. The current reference generation considering the current limits was investigated in [3, 15, 23], but the grid voltage limitation and the regulation of $\tilde{p}$, $\tilde{q}$ have not been discussed. In [24], although the regulation of $\tilde{p}$, $\tilde{q}$ was examined, the voltage and current limitation were not discussed. As shown in Table 4, the

$$I_{bmp} = \sqrt{\left[(g^+)^2 + (b^+)^2\right](V^+)^2 + \left[(k_G g^+)^2 + (k_B b^+)^2\right](V^-)^2 + 2\sqrt{(g^+)^2 + (b^+)^2}\sqrt{(k_G g^+)^2 + (k_B b^+)^2}V^+V^- \cos(\varphi_i^b)} \tag{32}$$

$$I_{cmp} = \sqrt{\left[(g^+)^2 + (b^+)^2\right](V^+)^2 + \left[(k_G g^+)^2 + (k_B b^+)^2\right](V^-)^2 + 2\sqrt{(g^+)^2 + (b^+)^2}\sqrt{(k_G g^+)^2 + (k_B b^+)^2}V^+V^- \cos(\varphi_i^c)} \tag{33}$$

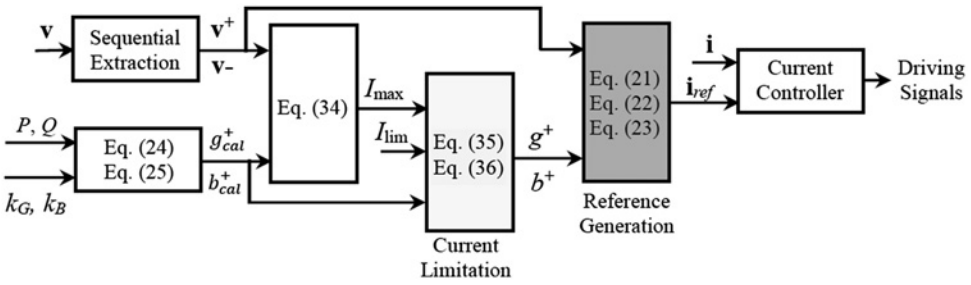

Fig. 5 *Current reference generation diagram*

Table 4 Comparison with the available schemes

Control schemes	Regulation of P, Q	Current limitation	Grid voltage limitation	Control of $\tilde{p}$, $\tilde{q}$
Ref. [12]	P	×	×	×
Ref. [13]		×	×	√
Ref. [16, 17]	Q	√	√	×
Ref. [3, 15, 23]	P and Q	√	×	×
Ref. [24]		×	×	√
Proposed PNGB		√	×	√

PNGB method proposed in this paper considers the regulation of $\tilde{p}$, $\tilde{q}$ and the current limitation, but the grid voltage is not discussed.

Main advantages of the proposed PNGB method include: (i) It enables the regulation of active and reactive power fluctuation to effectively minimise the active power oscillation, and (ii) achieves the current limitation control. Most existing power control techniques are not capable of achieving these two functionalities at the same time. Moreover, based on the analytical results obtained from Sections 2 and 3 and the decoupling characteristic of the proposed PNGB control method, the active power and reactive power fluctuation can be easily regulated through the control parameter k_G and k_B.

4 Numerical and experimental results

4.1 Numerical results

The numerical results mainly verify the quadrature characteristics of the active and reactive power ripple, and demonstrate that the average active and reactive powers P, Q affect the cosine term and the sine term independently.

The grid fault condition considered is the same as that used in Figs. 2 and 3. When $P = 500$ W, $Q = 500$ Var, $k_G = 0.5$, and $k_B = 0.5$, and the current limit is set to $I_{\lim} = 5$ A, waveforms of three-phase voltages and currents are shown in Fig. 6, so are the active power and reactive power oscillations. At this condition, the conductance is $g^+ = 0.01690$ and the susceptance is $b^+ = 0.01690$ according to (24) and (25). In the numerical simulation, the switching frequency ripple is ignored and the current control is assumed to accurately tracking the reference. The quadrature characteristics between $p_{\cos}$ and $p_{\sin}$, and between $q_{\cos}$ and $q_{\sin}$ components are observed, as evidenced by the dash-dot line in Figs. 6*c* and *d*.

Table 5 summaries the active power and reactive oscillations and the corresponding quadrature terms obtained by numerical simulation and analytical calculation. Three different power settings were considered. They are ($P = 500$ W, $Q = 500$ Var), ($P = 500$ W, $Q = 250$ Var), and ($P = 250$ W, $Q = 500$ Var). Results of the power ripples and the maximum phase current are also given in Table 5.

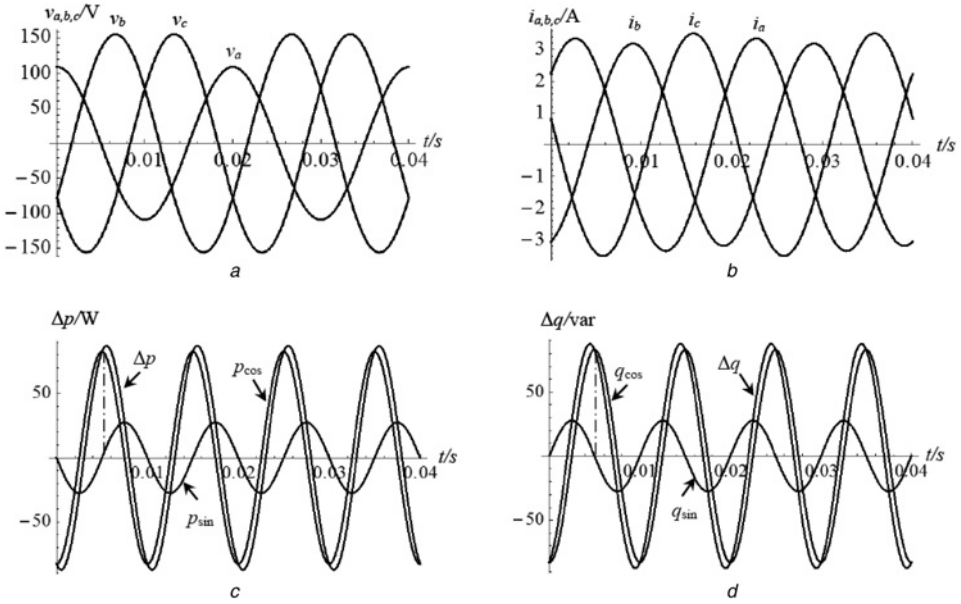

Fig. 6 *Simulation results for $P = 500$ W, $Q = 500$ Var, $k_G = 0.5$, and $k_B = 0.5$.*

a Three-phase voltage
b Three-phase currents
c Active power oscillation
d Reactive power oscillation

Table 5 Comparison of numerical simulation and analytical calculation under $k_G = 0.5$ and $k_B = 0.5$

P (W), Q (Var)		Δp_{cos}	Δp_{sin}	Δp	Δq_{cos}	Δq_{sin}	Δq	I_{max}, A
$P = 500$	num	82.29	27.34	87.37	82.24	27.45	87.02	3.52
$Q = 500$	cal	82.82	27.61	87.30	82.82	27.61	87.30	3.51
$P = 500$	num	82.83	14.06	83.87	41.32	27.57	49.42	2.78
$Q = 250$	cal	82.82	13.80	83.96	41.41	27.61	49.55	2.79
$P = 250$	num	41.43	27.58	49.93	82.78	13.84	84.03	2.75
$Q = 500$	cal	41.41	27.61	49.77	82.82	13.80	83.96	2.74

It can be seen from Table 5 that simulation results match well with the analytical results in all three cases. As pointed out in Section 2 that the average active power P determines the Δp_{cos} term and Δq_{sin} term independent of the average reactive power Q, while the average reactive power Q determines the Δp_{sin} term and Δq_{cos} term independent of the average active power P. This power characteristic is validated in Table 5. For example, for the power settings have the same average active power but different average reactive powers, the Δp_{cos} terms are nearly equal, the same holds for the Δq_{sin} term. On the other hand, for the power settings have the same average reactive powers, the Δp_{sin} terms are almost equal, so are the Δq_{cos} terms.

Next we examine the function of the current limitation control scheme. Fig. 7 presents the results with and without the proposed current control under unbalanced grid conditions. At the power setting of $P = 600$ W and $Q = 400$ Var, the current limit function was not triggered. When the current limit block does not function, simulation results are shown in Figs. 7*a*, *b*, *d* when power setting changes from $P = 600$ W and $Q = 400$ Var to $P = 1200$ W and $Q = 750$ Var. At this situation, g^+ and b^+ is changed from 0.02016 and 0.01343 to 0.04031 and 0.02520, respectively. The maximum phase current is 7.394 A, which is over the current limit 5 A when $P = 1200$ W and $Q = 750$ Var. When the current limitation block was functioning and simulation waveforms are shown in Figs. 7*c*, *e*. Then g^+ and b^+ is changed from 0.04031 and 0.02520 to 0.02726 and 0.01704, respectively, when the power setting is $P = 1200$ W and $Q = 750$ Var. The peak phase current is clamped to 5 A, while the average active power is limited to 827 W and the reactive power to 482 Var.

4.2 Experimental results

A three-phase three-wire VSC IGBT based prototype built in the lab was used for test. The current control is implemented by DSP 2812 in the stationary reference frame with proportional resonant regulator. The switching frequency is 10 kHz and the dc bus is fed

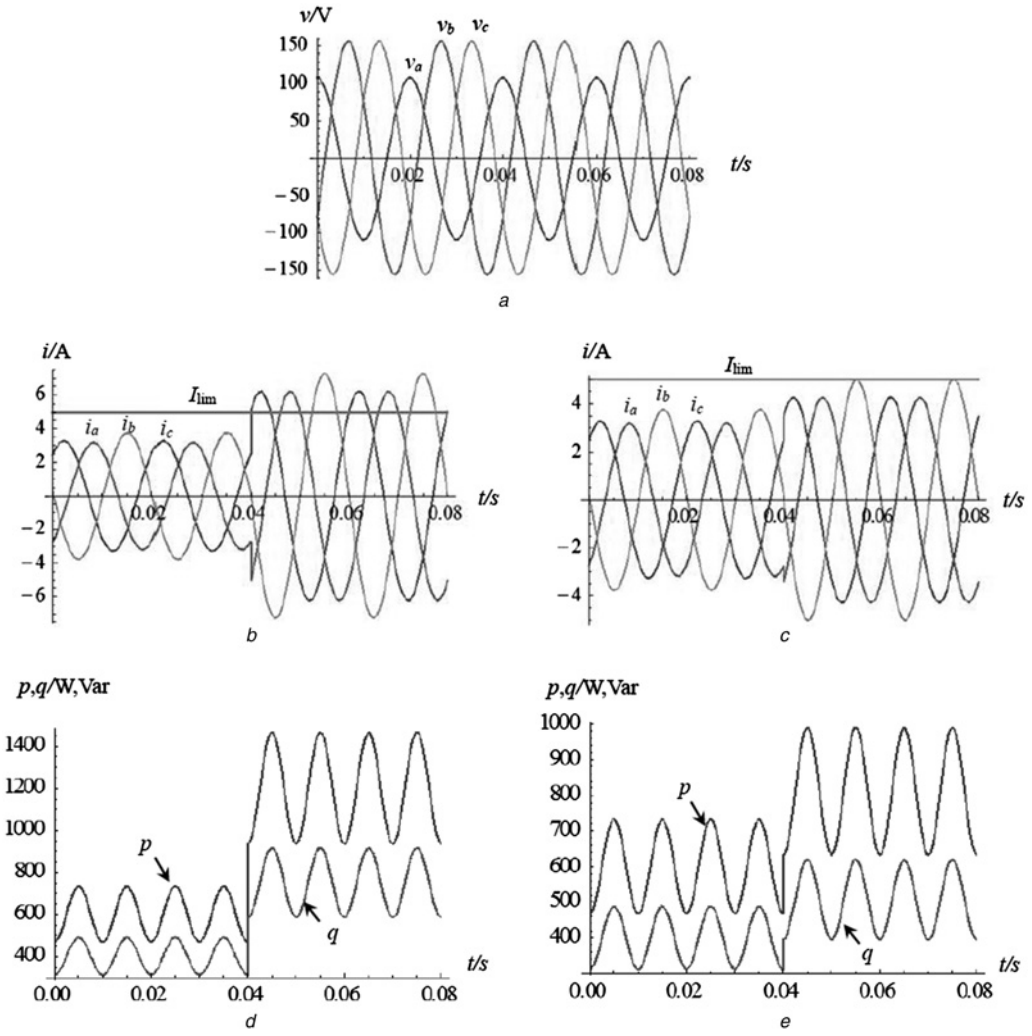

Fig. 7 *Simulation results on overcurrent limitation control*

a Three-phase voltage
b Three-phase current without current limit
c Three-phase current with current limit
d Instantaneous active and reactive power without current limit, and
e Instantaneous active and reactive power with current limit

IET Power Electron., 2016, Vol. 9, Iss. 11, pp. 2162–2173

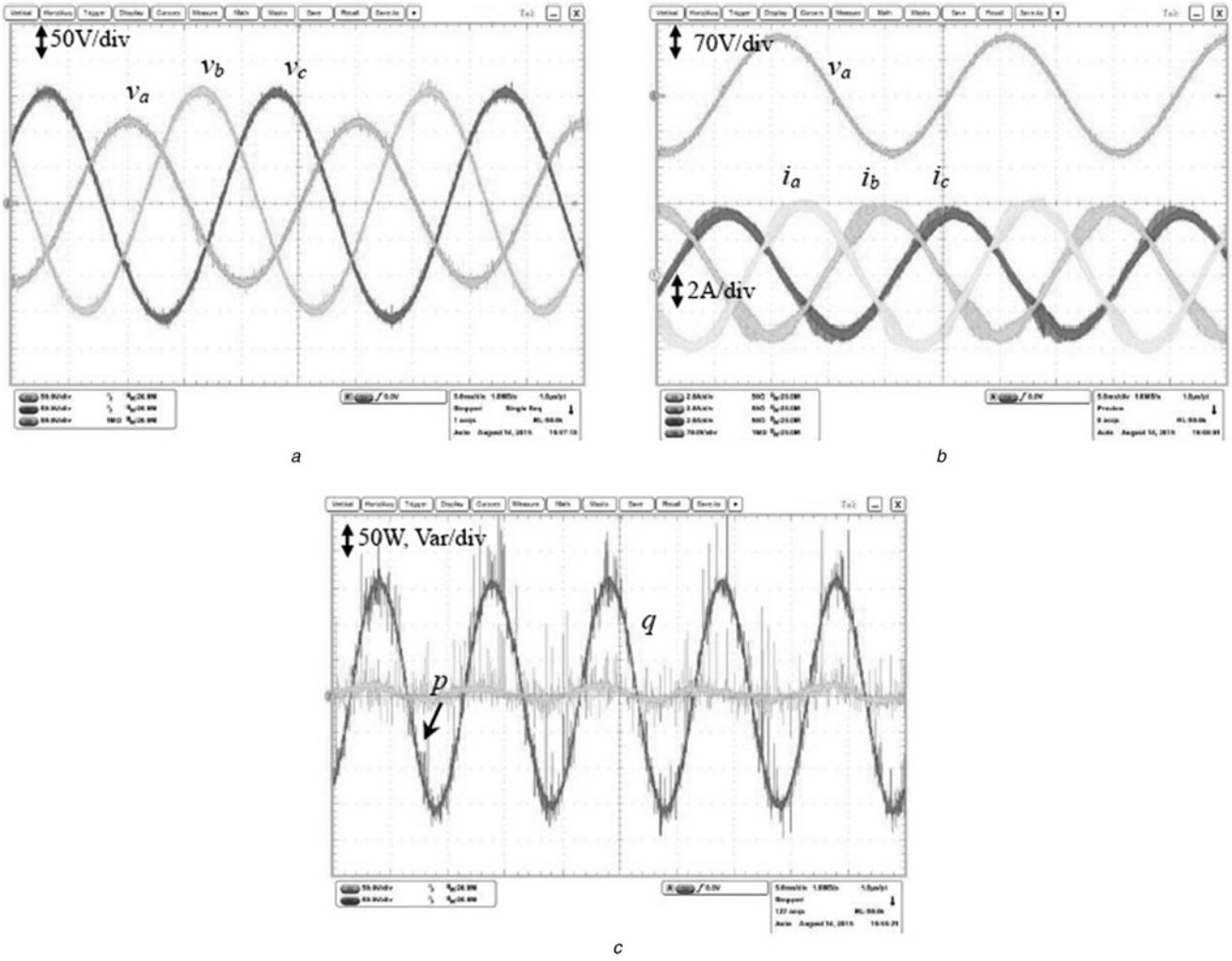

Fig. 8 *Experimental results when $P = 500$ W, $Q = 500$ Var, $k_G = -1$, and $k_B = 1$*

a Unbalanced three-phase voltage
b Unbalanced three-phase currents
c Instantaneous active and reactive power

by a 400 V dc source. The balanced condition was at 50 Hz and 110 V rms voltage. The grid fault condition was programmed by an AC source, and the fault condition was emulated with a 30% voltage drop in phase a. The current limit is set as 5 A in the experiment. The instantaneous active power and reactive power were calculated using the sampled voltage and current in DSP and sent out with a digital-analogue (DA) device. The probe gain of the oscilloscope is set to 1 V representing 1 W or 1 Var when measuring powers. The voltage and current were measured directly through voltage probe and current probe.

Several tests have been conducted to verify the effectiveness on minimisation of active power oscillation through the PNGB method, and to validate the current limitation control scheme. Four power settings were considered. Power setting 1 is for $P = 500$ W, $Q = 500$ Var, power setting 2 for $P = 600$ W, $Q = 400$ Var, power setting 3 for $P = 1000$ W, $Q = 1000$ Var, and power setting 4 for $P = 1200$ W, $Q = 750$ Var.

4.2.1 Minimisation of active power oscillation: As indicated in (26), when $k_G = -1$ and $k_B = 1$, the active power oscillation can be minimised to zero. According to (27), the control target is to achieve the active power oscillation of 0 W and the reactive power ripple of 157.18 Var for power setting 1. For power setting 2, the control target is to achieve the active power oscillation of 0 W and the reactive power ripple of 161 Var.

Two experiments were conducted using $k_G = -1$ and $k_B = 1$ and with power setting 1 and power setting 2. Fig. 8 shows the experimental results of power setting 1, and Fig. 9 illustrates the results of power setting 2. Both figures show that three-phase currents are unbalanced under these two power settings. It is observed from Fig. 8 that, the active power has small ripple of size up to 8 W, and the reactive power has quite large ripple of size of 158 Var. Fig. 9 shows that the measured active power ripple is 9.6 W and the reactive power ripple is 165.4 Var. It is also observed from Figs. 8 and 9 that the peak phase currents are 3.74 and 3.98 A for the power settings 1 and 2, respectively. Both currents are lower than the current limit set as 5 A in the experiment. Hence the current limitation control does not take effect.

4.2.2 Current limitation control: The current limitation control performance is evaluated experimentally in this section. Consider the situation of $k_G = 1$ and $k_B = 1$. The peak current calculated from (34) is 3.651 A for power setting 1, and is 7.5 A for power setting 3 without current limitation. Fig. 10 exhibits the current limitation control performance when the power setting is changed from 1 to 3. Figs. 10*a* and *b* show the waveforms of three-phase voltage, currents, and the corresponding instantaneous active power and reactive power without current limitation control, and Figs. 10*c* and *d* with current limitation control. It is observed from Fig. 10*a* that, with no current control, the maximum peak current changes

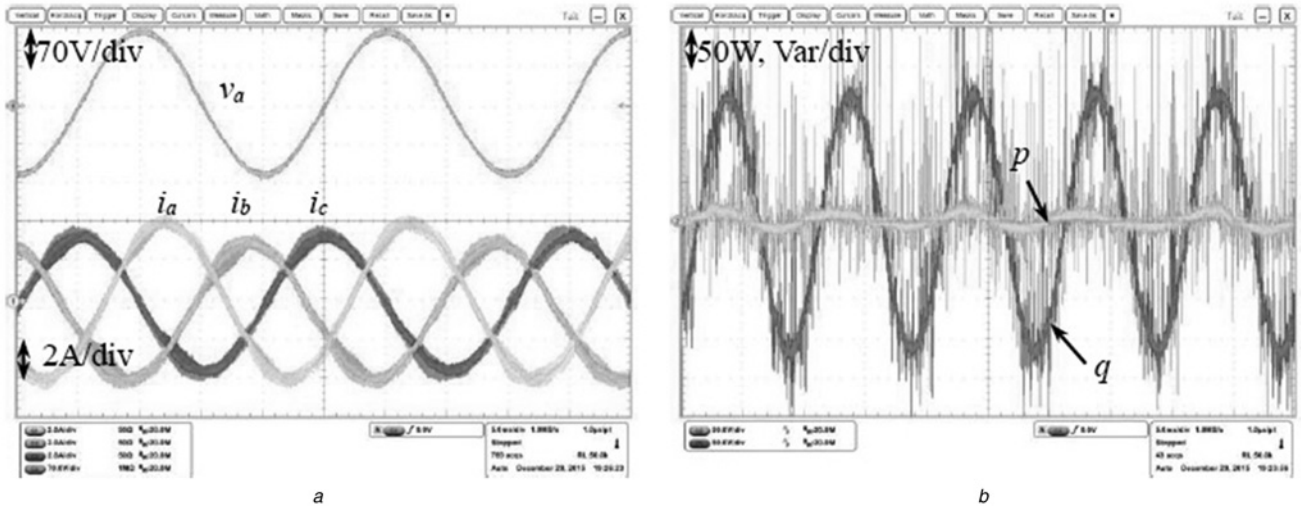

Fig. 9 *Experimental results when P = 600 W, Q = 400 Var, $k_G = -1$, and $k_B = 1$*

a Unbalanced three-phase currents
b Instantaneous active and reactive power oscillation

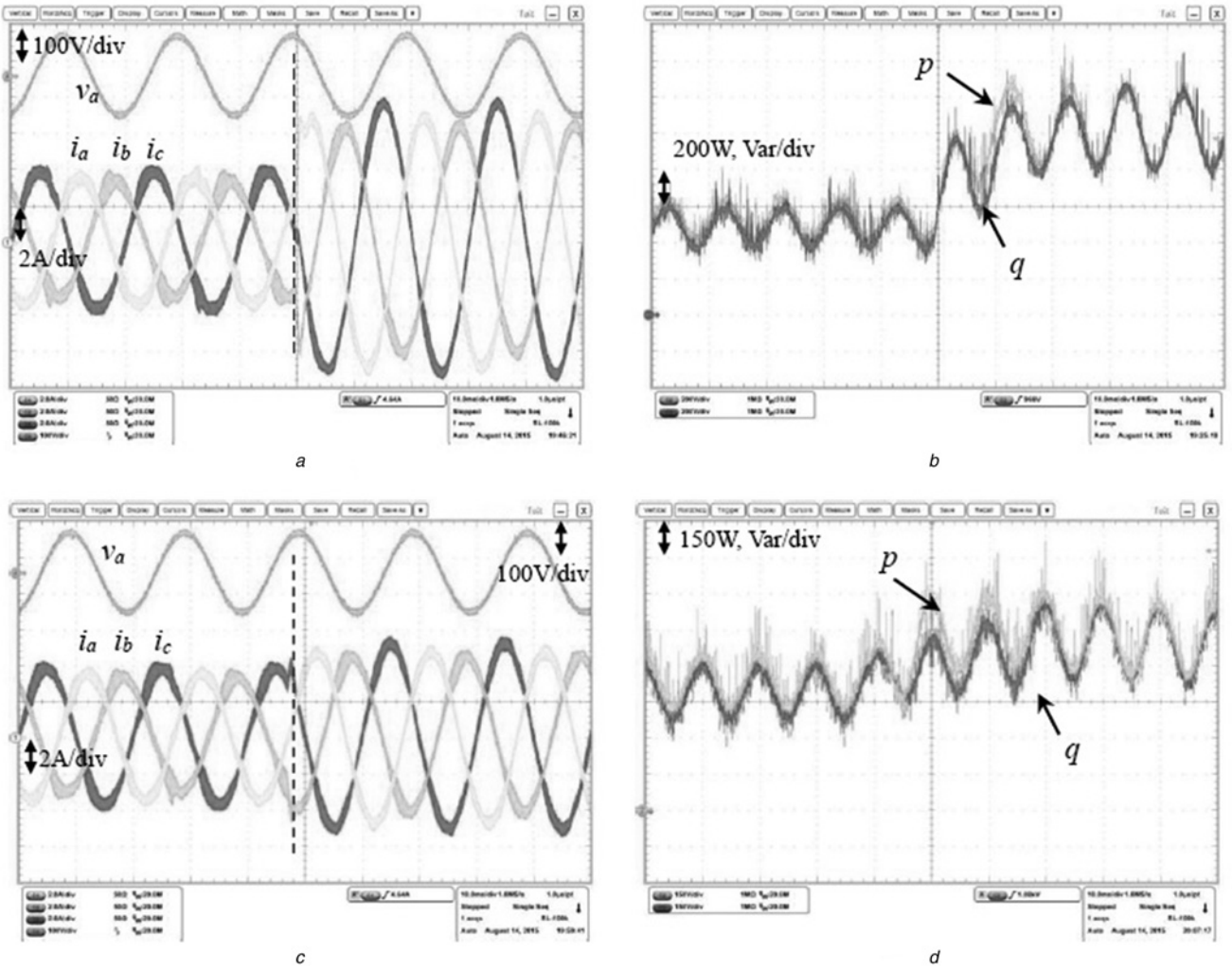

Fig. 10 *Effect of the proposed current limitation control scheme. The vertical dash line indicates the time the power setting is changed from power setting 1: P = 500 W, Q = 500 Var to power setting 2: P = 1000 W, Q = 1000 Var. Grid voltage and three-phase currents*

a Without and *c* with current limitation control. Instantaneous active power and reactive power
b Without
d With current limitation control

IET Power Electron., 2016, Vol. 9, Iss. 11, pp. 2162–2173

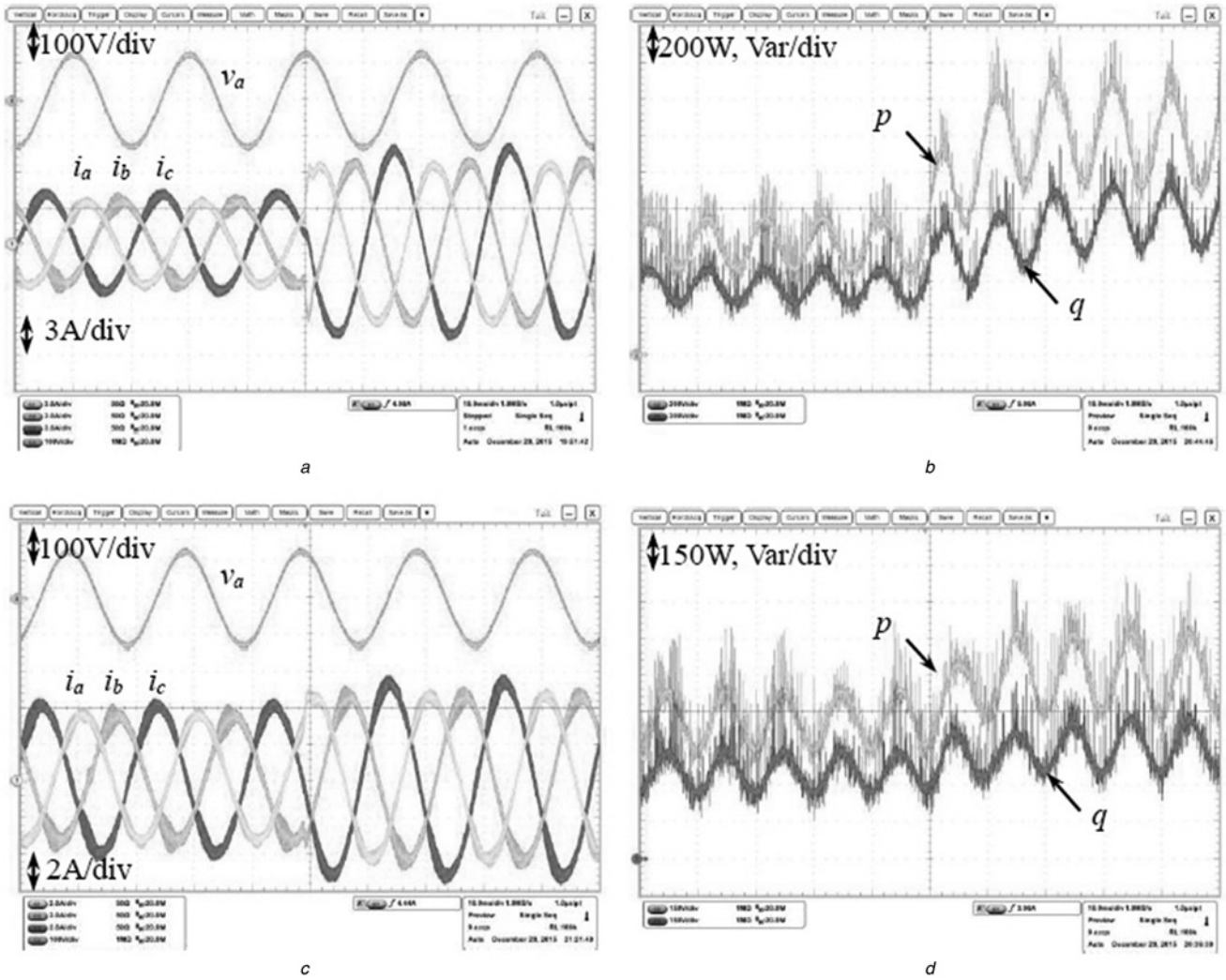

Fig. 11 *Effect of the proposed current limitation control scheme. Power is changed from P = 600 W, Q = 400 Var to P = 1200 W, Q = 750 Var. Grid voltage and three-phase currents*

a Without and *c* with current limitation control; instantaneous active power and reactive power
b Without and
d With current limitation control

from 3.79 to 7.45 A, whereas it changes from 3.79 to 5.11 A when the current limitation control is applied, as evidenced from Fig. 10*c*.

Other benefits of current limitation control include the following. The conductance g^+ is limited to 0.02301 from 0.03360 at power setting 3. Similarly, the susceptance b^+ is limited to 0.02301 instead of 0.03360. The current limitation control scheme also lowers the active and reactive power from $P = 1000$ W and $Q = 1000$ Var to 704 W and 692 Var, respectively. Furthermore, the magnitude of the active power ripple is down from 215 to 146 W, as shown in Figs. 10*b* and *d*. Similar performance was also observed for the reactive power.

Another current limitation control test for $k_G = 1$ and $k_B = 1$ is to change the power setting from $P = 600$ W, $Q = 400$ Var to $P = 1200$ W and $Q = 750$ Var. Experimental results are shown in Fig. 11. When the current limitation control is not activated, the maximum peak current is changed from 3.94 to 7.56 A as shown in Fig. 11*a*. When the current limitation control kicks in, Fig. 11*c* shows that the maximum peak current becomes 5.20 A. At power setting 4, the conductance g^+ is limited to 0.02726 from 0.04031, and the susceptance b^+ is limited to 0.01704 instead of 0.02520. The current limit control scheme also lowers the active power from $P = 1200$ W to 793 W and the reactive power from $Q = 750$ Var and 482 Var. In addition, the current limitation control enables the magnitude of the active power ripple reduced from 276.8 W in Fig. 11*b* to 172.7 W in Fig. 11*d*. The reactive power ripple is also lowered from 159.3 to 111 Var.

5 Reactive power output capability

This section analyses the reactive power output capability of the proposed control scheme under voltage sag.

Consider the single-phase grounded fault in per-unit. Suppose that the voltage sag occurs at phase *a* and its amplitude is dropped to k ($0 \le k \le 1$). Then the three phase voltages are

$$\begin{cases} v_a = k\ \cos(t) \\ v_b = \cos\left(t - \dfrac{2}{3}\right) \\ v_c = \cos\left(t + \dfrac{2}{3}\right). \end{cases} \tag{37}$$

It can be shown [8] that amplitudes of the positive sequence voltage V^+ and the negative sequence voltage V^- can be expressed as

$$\begin{cases} V^+ = \dfrac{k+2}{3} \\ V^- = \dfrac{1-k}{3}. \end{cases} \tag{38}$$

If we set the current limit to 1.0 per unit when the conventional maximum reactive power output is set, then the maximum reactive

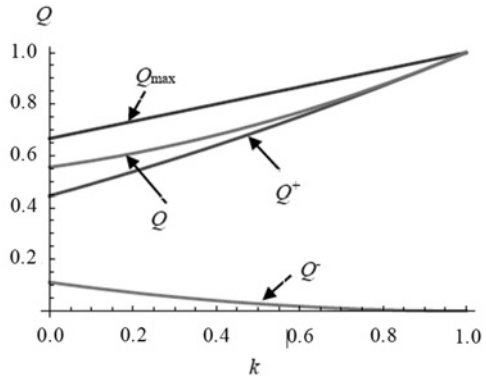

Fig. 12 *Reactive power output capability versus the sag depth*

power output will be

$$Q_{\max} = \frac{k+2}{3}. \tag{39}$$

If the control scheme is set to maximally compensate the reactive power and to realise zero $\tilde{p}$, then it follows from (26) that $g^+ = 0$ and $k_B = 1$ when the PNGB control scheme is applied. The maximum positive and negative sequence currents are, respectively, $I^+ = (k+2)/3$ and $I^- = (1-k)/3$ so that the maximum current $I_{\max}$ limit of (34) is satisfied. The maximum positive and negative sequence reactive powers Q^+, Q^- and their sum Q can be generated by

$$Q^+ = \left(\frac{k+2}{3}\right)^2 \tag{40}$$

$$Q^- = \left(\frac{k-1}{3}\right)^2 \tag{41}$$

$$Q = \left(\frac{k+2}{3}\right)^2 + \left(\frac{k-1}{3}\right)^2. \tag{42}$$

The reactive power output capability is illustrated in Fig. 12, which depicts the relationship of reactive power output and the degree of voltage sag. The reactive power output by the proposed control scheme is characterised by Q of (42), while that by the traditional control methods is characterised by $Q_{\max}$ of (39). At the worst scenario of $k = 0$, the phase a voltage drops to 0, the reactive power capability of the traditional method is $Q_{\max} = 0.667$. For the presented method, the positive sequence reactive power is $Q^+ = 0.444$ and the negative sequence reactive power is $Q^- = 0.111$ for a total of $Q = 0.555$. It can be concluded that the reduction of the active power fluctuation is at the cost of the decrease of the maximum reactive power capability. For other types of grid faults, similar process can be taken to analyse the reactive power output capability.

6 Conclusions

This paper presents the analysis of instantaneous active and reactive power oscillation of three-phase grid-connected VSC. The results have shown that the quadrature characteristics of the active and reactive power oscillation results in the cosine term and the sine term representations which are solely determined, respectively, by the average active power and the average reactive power. A PNGB current control method has been proposed to regulate the instantaneous active and reactive power oscillation. Moreover, a current limitation scheme is embedded into the control loop to prevent the overcurrent. Simulation and experimental results have validated the analysis of power oscillation and demonstrate the effectiveness of the proposed control scheme. These findings shed insight on the oscillation power under unbalanced grid conditions, and along with the current limitation scheme, can be used as the design reference of other control schemes under unbalanced grid conditions.

7 Acknowledgment

This work was supported in part by the Natural Science Foundation Project of CQ CSTC under grant no. CSTC2012JJJQ90004, the National Natural Science Foundation of China under grant no. 51137006, the Fundamental Research Funds for the Central Universities under grand no. CDJZR14158801 and the State Grid Project grand no. SGCQDK00PJJS1500069.

8 References

1 Song, H., Nam, K.: 'Dual current control scheme for PWM converter under unbalanced input voltage conditions', *IEEE Trans. Ind. Electron.*, 1999, **46**, (5), pp. 953–959
2 Blaabjerg, F., Teodorescu, R., Liserre, M., *et al.*: 'Overview of control and grid synchronization for distributed power generation systems', *IEEE Trans. Ind. Electron.*, 2006, **53**, (5), pp. 1398–1409
3 Camacho, A., Castilla, M., Miret, J., *et al.*: 'Active and reactive power strategies with peak current limitation for distributed generation inverters during unbalanced grid faults', *IEEE Trans. Ind. Electron.*, 2015, **62**, (3), pp. 1515–1525
4 Neves, F.A.S., Carrasco, M., Mancilla-David, F.G., *et al.*: 'Unbalanced grid fault ride–through control for single–stage photovoltaic inverters', *IEEE Trans. Power Electron.*, 2016, **31**, (4), pp. 3338–3347
5 Ng, C., Ran, L.: 'Unbalanced-grid-fault ride-through control for a wind turbine inverter', *IEEE Trans. Ind. Appl.*, 2008, **44**, (3), pp. 845–856
6 Tsili, M., Papathanassiou, S.: 'A review of grid code technical requirements for wind farms', *IET Renew. Power Gener.*, 2009, **3**, (3), pp. 308–332
7 'The grid code, issue 3, rev. 24' National Grid Electricity Transmission plc, UK, October 2008
8 Andersson, P.M.: 'Analysis of faulted power systems' (IEEE Press, New York, 1995)
9 Moran, L., Ziogas, P.D., Joos, G.: 'Design aspects of synchronous PWM rectifier-inverter systems under unbalanced input voltage conditions', *IEEE Trans. Appl.*, 1992, **28**, (6), pp. 1286–1293
10 Mirhosseini, M., Pou, J., Agelidis, V.G.: 'Individual phase current control with the capability to avoid overvoltage in grid-connected photovoltaic power plants under unbalanced voltage sags', *IEEE Trans. Power Electron.*, 2015, **30**, (10), pp. 5346–5351
11 European Network of Transmission System Operator (ENTSO): 'Entso-e draft network code for requirements for grid connection applicable to all generators [Online]'. January 2012, Available at https://www.entsoe.eu/ major-projects/network-code-development/requirements-for-generators/Pages/default.aspx
12 Rodriguez, P., Timbus, A., Teodorescu, R., *et al.*: 'Flexible active power control of distributed power generation systems during grid faults', *IEEE Trans. Ind. Electron.*, 2007, **54**, (5), pp. 2583–2592
13 Castilla, M., Miret, J., Sosa, J.L., *et al.*: 'Grid-fault control scheme for three-phase photovoltaic inverters with adjustable power quality characteristics', *IEEE Trans. Power Electron.*, 2010, **25**, (12), pp. 2930–2940
14 Alepuz, S., Monge, S., Bordonau, J., *et al.*: 'Control strategies based on symmetrical components for grid-connected converters under voltage dips', *IEEE Trans. Ind. Electron.*, 2009, **56**, (6), pp. 2162–2173
15 Camacho, A., Castilla, M., Miret, J., *et al.*: 'Flexible voltage support control for three phase distributed generation inverters under grid fault', *IEEE Trans. Ind. Electron.*, 2013, **60**, (4), pp. 1429–1441
16 Camacho, A., Castilla, M., Miret, J., *et al.*: 'Reactive power control for distributed generation power plants to comply with voltage limits during grid faults', *IEEE Trans. Power Electron.*, 2014, **29**, (11), pp. 6224–6234
17 Miret, J., Camacho, A., Castilla, M., *et al.*: 'Reactive current injection protocol for low power rating distributed generation sources under voltage sags', *IET Power Electron.*, 2015, **8**, (6), pp. 879–886
18 Guo, X., Zhang, X., Wang, B., *et al.*: 'Asymmetrical grid fault ride-through strategy of three-phase grid-connected inverter considering network impedance impact in low-voltage grid', *IEEE Trans. Power Electron.*, 2014, **29**, (3), pp. 1064–1068
19 Lee, C., Hsu, C., Cheng, P.: 'A low-voltage ride-through technique for grid-connected converters of distributed energy resources', *IEEE Trans. Ind. Appl.*, 2011, **47**, (4), pp. 1821–1832
20 Miret, J., Castilla, M., Camacho, A., *et al.*: 'Control scheme for photovoltaic three-phase inverters to minimize peak currents during unbalanced grid-voltage sags', *IEEE Trans. Power Electron.*, 2012, **27**, (10), pp. 4262–4271
21 Ma, K., Chen, W., Liserre, M., *et al.*: 'Power controllability of a three-phase converter with an unbalanced AC source', *IEEE Trans. Power Electron.*, 2015, **30**, (3), pp. 1591–2603
22 Roscoe, A.J., Finney, S., Burt, G.M.: 'Tradeoffs between AC power quality and DC bus ripple for 3-phase 3-wire inverter-connected devices within microgrids', *IEEE Trans. Power Electron.*, 2011, **26**, (3), pp. 674–688

23 Rodriguez, P., Luna, A., Etxeberria-Otadui, I., *et al*.: 'Current control method for distributed generation power generation plants under grid fault conditions'. Proc. 37th Int. Annual Conf. IEEE Industrial Electronics Society (IECON), Melbourne, VIC, November 2011, pp. 1262–1269
24 Wang, F., Duarte, J.L., Hendrix, M.: 'Pliant active and reactive power control for grid interactive converters under unbalanced voltage dips', *IEEE Trans. Power Electron.*, 2011, **26**, (5), pp. 1511–1521
25 Akagi, H., Watanabe, E.H., Aredes, M.: 'Instantaneous Power Theory and Applications to Power Electronics' (John Wiley & Sons Inc., Hoboken, New Jersey, 2007), Chapter 3, pp. 74–75
26 Rodriguez, P., Luna, A., Munoz-Aguilar, R.S., *et al*.: 'A stationary reference frame grid synchronization system for three-phase grid-connected power converters under adverse grid conditions', *IEEE Trans. Power Electron.*, 2012, **27**, (1), pp. 99–112